Cascode Connected AlGaN/GaN HEMT's on SiC Substrates

Bruce M. Green, *Student Member IEEE*, Kenneth K. Chu, Joseph A. Smart, Vinayak Tilak, Hyungtak Kim, *Student Member, IEEE*, James R. Shealy, and Lester F. Eastman, *Life Fellow, IEEE*

***Abstract*—We report on the fabrication and characteristics of cascode-connected AlGaN/GaN HEMT's. The HEMT's were realized using $Al_{0.3}Ga_{0.7}N$/GaN heterostructures grown on 6-H semi-insulating SiC substrates. The circuit reported here employs a common source device having a gate length of 0.25 μm cascode connected to a 0.35 μm common gate device. The gate width of each device is 250 μm. The fabricated circuit exhibited a current density of 800 mA/mm and yielded an f_T and $f_{\max}$ of 24.5 and 56 (extrapolated) GHz, respectively. Large signal measurements taken at 4 GHz produced 4 W/mm saturated output power at 36% power-added efficiency. Comparisons to the performance of a 250×0.35 μm^2 common source device taken from the same wafer show that the cascode configuration has 7 dB more linear gain and 3 dB more compressed gain than the common source device at 4 GHz.**

***Index Terms*—Cascode, GaN, HEMT's, SiC.**

I. Introduction

PROGRESS in the materials growth and device processing technologies for AlGaN/GaN HEMT's on SiC substrates have increased the state-of-the-art for microwave transistor power densities to powers in excess of 9 W/mm at X band for devices grown on SiC substrates [1]. Previously, GaN-based dual gate HEMT's and flip-chip bonded broadband amplifier circuits based on HEMT's grown on sapphire substrates have been reported [2], [3]. This letter presents the dc, small signal, and power characteristics of cascode-connected AlGaN/GaN HEMT's on SiC substrates. The higher thermal conductivity of SiC (≈3.4 W/cm-K) compared to sapphire (≈ 0.4W/cm-K) makes this the substrate of choice for AlGaN/GaN HEMT MMIC applications. Cascode circuits find wide application in microwave amplifiers [4], phase shifters [5], and pre-distorters [6]. This paper presents dc, small signal, and CW power results for 250 μm cascode-connected HEMT's on SiC substrates. Power densities of 4 W/mm (1 W total power) at 4 GHz were achieved with an associated linear gain of 22 dB. Comparative data for a 250×0.35 μm^2 device show that the cascode configuration produces an additional 7 dB linear gain and an additional 3 dB gain at saturation.

Manuscript received April 10, 2000; revised May 31, 2000. This work was supported by the ONR MURI Program uncer Contract N00014-96-1-1223 monitored by Dr. J. C. Zolper.

B. M. Green, J. A. Smart, V. Tilak, H. Kim, J. R. Shealy, and L. F. Eastman are with the School of Electrical and Computer Engineering, Cornell University, Ithaca, NY 14853 USA.

K. K. Chu was with the School of Electrical and Computer Engineering, Cornell University, Ithaca, NY 14853 USA. He is now with GE Corporate Research and Development, Schenectady, NY 12301 USA.

Publisher Item Identifier S 1051-8207(00)07041-0.

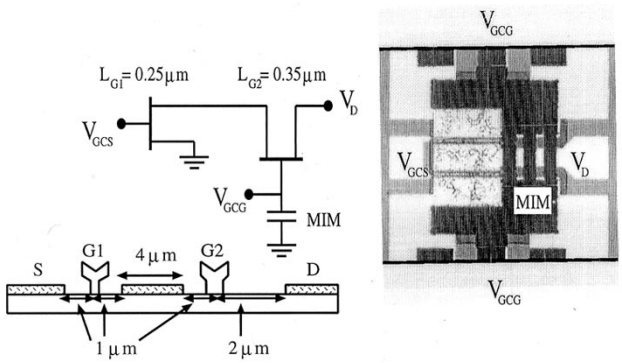

Fig. 1. Schematic digram, device cross section, and die photo of fabricated 250 μm cascode connected HEMT's. Note that all gate-ohmic distances are given from the gate center.

II. Cascode Connected HEMT Design and Fabrication

The design of the cascode connected HEMT schematically shown in Fig. 1 employs a short gate ($L_g = 0.25$ μm) common source device (CS) optimized for high current gain and high f_T cascode connected to a longer gate ($L_g = 0.35$ μm) common gate (CG) device optimized for high breakdown voltage. For class A operation, the maximum gate-drain voltage on the common source device occurs during the pinched off portion of the RF cycle. Its value is given by

$$V_{\max, G-D} = V_{G2, DC} - V_{T, CS} - V_{T, CG} \tag{1}$$

where $V_{T, CS}$, $V_{T, CG}$, refer to the threshold voltages of the common source and common gate devices, respectively, and $V_{G2, DC}$ refers to the dc bias voltage applied to the common gate device. For these devices in typical large signal operation, $V_{T, CS} \approx V_{T, CG} = -5$ V and $V_{G2, DC} = 3 - 5$ V. Therefore, the maximum value of $V_{\max, G-D}$ is 13–15 V. Because of this, even shorter gate lengths could be used for the common source device since the AlGaN/GaN HEMT's with 0.25 μm gate lengths are typically able to withstand gate-drain voltages in excess of 30 V. A 0.25 μm gate length was used in this study to ensure reproducibility and device yield. As shown in Fig. 1, 1 μm gate-source and gate-drain spacings for the common gate device were chosen to minimize the source resistance and knee voltage. The common-gate device was designed to have a 0.35 μm gate length and a 2 μm gate-drain spacing (L_{G-D}) for further optimization of the gate-drain breakdown voltage. Unlike a classical dual gate FET where the gates of the CS and CG device have a pitch on the order 1 μm, the CS and CG devices are separated by

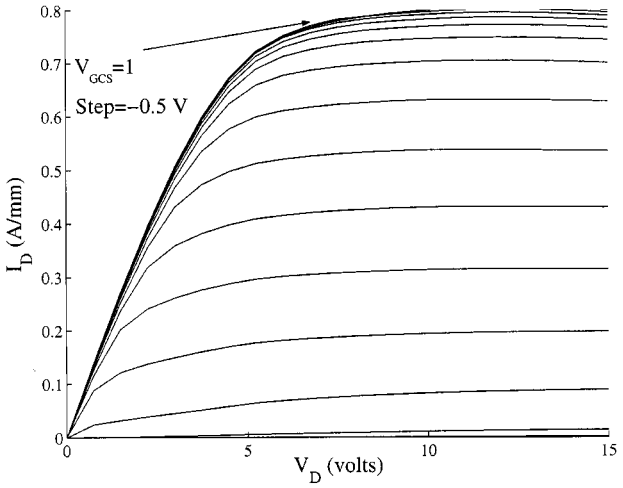

Fig. 2. Measured dc curves for 250 μm cascode connected HEMT ($V_{GCG=0}$ V).

a 4 μm wide strip of ohmic contact metalization. This metalization provides a low-resistance cascode connection of the devices while allowing the devices to operate as two cascode-connected transistors with no interaction between the depletion regions of the devices. Such a configuration has been used in other applications where it was desired to have a definite separation between the two devices while maintaining a low interconnect resistance [4]. Two of these cascode connected sets of gate fingers with a finger length of 125 μm are separated by a distance of 50 μm to form a 250 μm cascode cell.

Using these design guidelines, the cascode circuits were fabricated. Details concerning materials growth, mesa etching, ohmic contact formation, and e-beam gate lithography may be found in [7]–[9]. Here, device passivation and dielectric deposition for high breakdown voltage MIM capacitors is accomplished using a 350 nm thick layer of Si_3N_4. The top plates of the MIM capacitors and airbridges are formed using gold plated to a thickness of 2.5 μm. A micrograph of the finished device with accompanying MIM capacitor, common-gate biasing pads and input/output pads is shown in Fig. 1. The contact for the common source device is accessed at the left. Airbridges connecting symmetrical MIM capacitors at the top and bottom provide a dc connection to the gate of the common gate device.

III. DC and Small Signal Characteristics

Fig. 2 shows dc curves produced by the fabricated cascode-connected HEMT with 0 V on the common gate terminal of the fabricated devices. S-parameter measurements of the cascode-connected HEMT were performed over 1–26.5 GHz with $+3$ V on the common gate terminal, -3.4 V on the gate, and 20 V on the drain. For the purposes of comparison, S parameter measurements were also made on common source devices of the same cross-sectional geometry used for the common gate device in the cascode circuit ($L_g = 0.35$ μm, $L_{G-D} = 2$ μm). A bias of -3.5 V on the gate and 10 V on the drain were applied. As can be seen from Fig. 3 comparing the maximum stable gain (MSG)/maximum available gain

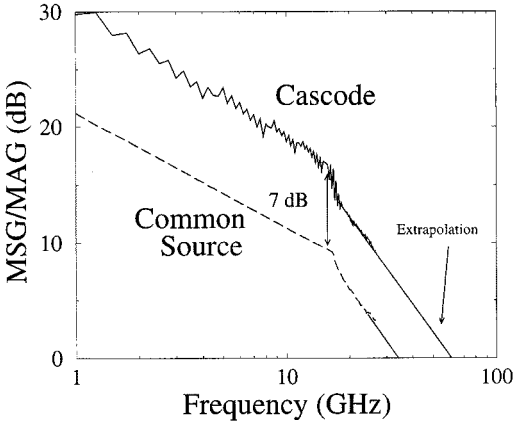

Fig. 3. Comparison of maximum stable gain (MSG)/ maximum available gain (MAG) for 250 μm cascode connected HEMT's and 250×0.35 μm^2 common source device.

(MAG) for the casode and common source devices, the cascode configuration exhibits 7 dB more stable gain than the common source device with an increase in $f_{\max}$ from 34 to 56 GHz. However, a decrease was seen in f_T from 28 GHz to 24.5 GHz for the cascode configuration compared to the common source device. This decrease in f_T compared to the common source device can be understood by noting the additional pole in the simplified expression for the current gain for the cascode configuration given by

$$h_{21,CC}(f) \approx \frac{1}{\left(1 - \dfrac{f}{jf_{T,CG}}\right)\dfrac{f}{jf_{T,CS}}}. \tag{2}$$

Here, $f_{T,CG}$ and $f_{T,CS}$ refer to the cutoff frequencies of the common gate and common source devices, respectively. Using this result and the measured f_T's of the common gate and common source devices (28 GHz and 34 GHz), an overall f_T of 25 GHz is obtained, which is very close to the measured value.

IV. Large Signal Characterization

On-wafer power measurements of the cascode-connected HEMT's of this study were performed using a Focus Microwaves™ loadpull system. Fig. 4(a) shows power sweep data for 250 μm cascode-connected HEMT's at 4 GHz. For this measurement, the bias conditions were set at $V_D = 25$ V, $V_{GCG} = 5$ V, and $V_{GCS} = -4$ V. As seen from the figure, the cascode configuration produced 4 W/mm (1 W total power) with associated saturated gain and power-added-efficiency (PAE) of 13 dB and 35%, respectively. The associated source and load impedances were $61 + j115\ \Omega$ and $88 + j76\ \Omega$, respectively. A 250×0.35 μm^2 common source device from the same wafer yielded 4 W/mm with an associated gain and power-added efficiency (PAE) of 10 dB and 30%, respectively, as shown in Fig. 4(b) ($Z_S = 84 + j115\ \Omega$, $Z_L = 120 + j30\ \Omega$).

V. Discussion and Conclusion

Characteristics of cascode connected AlGaN/GaN HEMT's on SiC substrates have been presented. It should be noted that the results for this cascode circuit may be scaled to devices

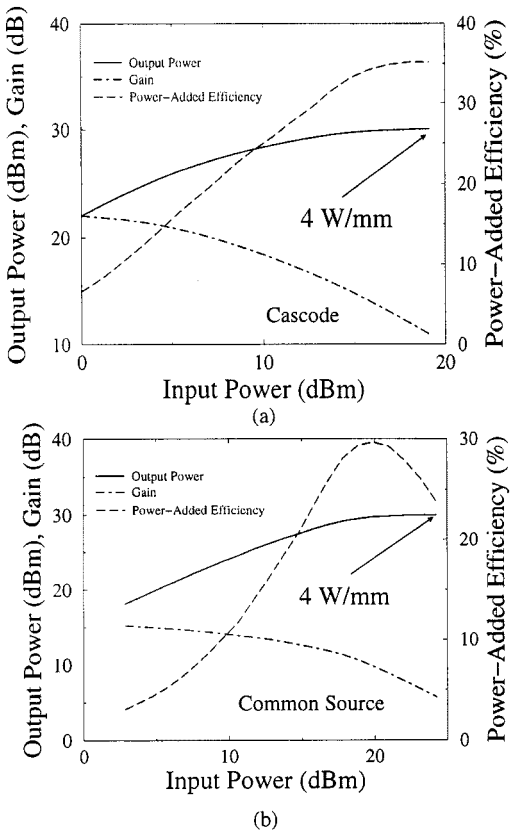

Fig. 4. Power saturation characteristics for (a) 250 μm cascode device ($f = 4$ GHz, $V_D = 25$ V, $V_{GCS} = -4$ V, $V_{GCG} = 5$ V) compared to (b) saturation characteristics for 250×0.35 μm^2 common source device ($f = 4$ GHz, $V_D = 25$ V, $V_G = -4$ V).

of larger peripheries since the thermal limit of 17 W/mm of heat dissipation allowed for large, multi-finger devices on 330 μm thick SiC substrates has not been reached [10]. Common source devices with total gate peripheries up to 1 mm were measured at 4 GHz and also exhibited 4 W/mm with only a small loss in gain due to the distributed effects of the device. It is expected that improvements in materials growth and process technology of the devices will raise the 45 V gate-source breakdown voltage currently limiting the power density (4 W/mm) and PAE (30%) of the common source devices. Nonetheless, these results show the viability of AlGaN/GaN/SiC technology for MMIC applications.

REFERENCES

[1] Y.-F. Wu, D. Kapolnek, J. Ibbetson, N.-Q. Zhang, P. Parikh, B. P. Keller, and U. K. Mishra, "High Al-content AlGaN/GaN HEMT's on SiC substrates with very high power performance," in *IEDM Tech. Dig.*, Washington, DC, Dec. 1999, pp. 925–927.

[2] C. H. Chen, K. Krishamurthy, S. Keller, G. Parish, M. Rodwell, U. K. Mishra, and Y. F. Wu, "AlGaN/GaN dual-gate modulation-doped field-effect transistors," *Electron. Lett.*, vol. 35, pp. 933–935, May 1999.

[3] J. J. Xu, Y. F. Wu, S. Keller, S. Heikman, B. J. Thibeault, U. K. Mishra, and R. A. York, "1–8 GHz GaN-based power amplifier using flip-chip bonding," *IEEE Microwave Guided Wave Lett.*, vol. 9, pp. 277–279, July 1999.

[4] M. Schlechtweg, W. H. Haydl, A. Bangert, J. Braunstein, P. J. Tasker, L. Verweyen, H. Massler, W. Bronner, A. Hulsmann, and K. Kohler, "Coplanar millimeter-wave IC's for W-band applications using 0.15 μm pseudomorphic MODFET's," *IEEE J. Solid State Circuits*, vol. 31, pp. 1426–1434, Oct. 1996.

[5] J. L. Vorhaus, R. A. Pucel, and Y. Tajima, "Monolithic dual-gate FET digital phase shifters," *IEEE Trans. Microwave Theory Tech.*, vol. MTT-30, pp. 982–991, 1982.

[6] M. Kumar, "Pre-distortion linearizer using GaAs dual-gate MESFETs for TWTA and SSPA used in sattllite transponders," *IEEE Trans. Microwave Theory Tech.*, vol. MTT-33, pp. 1479–1488, Dec. 1985.

[7] J. A. Smart, A. T. Schremer, N. G. Weimann, O. Ambacher, L. F. Eastman, and J. R. Shealy, "AlGaN/GaN heterostructures on insulating AlGaN nucleation layers," *Appl. Phys. Lett.*, vol. 75, no. 3, pp. 388–390, July 19, 1999.

[8] K. K. Chu, J. A. Smart, J. R. Shealy, and L. F. Eastman, "AlGaN/GaN piezoelectric HEMT's with submicron gates on sapphire," in *Proc. State-of-the-Art Program on Compound Semiconductors (SOTAPOCS) XXIX*, 1998.

[9] B. M. Green, K. K. Chu, E. M. Chumbes, J. A. Smart, J. R. Shealy, and L. F. Eastman, "The role of surface passivation on the microwave characteristics of AlGaN/GaN HEMT's," *IEEE Electron Device Lett.*, vol. 21, pp. 268–270, June 2000.

[10] L. F. Eastman and N. G. Weimann, "private communication," unpublished.